

Tunnelling of a composite particle in presence of a magnetic field

B Faulend, J Dragašević

Department of Physics, Faculty of Science, University of Zagreb, Zagreb, Croatia

E-mail: bfaulend@yahoo.com, jan.dragasevic@gmail.com

Abstract.

We present a simple model of composite particle tunnelling through a rectangular potential barrier in presence of magnetic field. The exact numerical solution of the problem is provided and the applicability to real physical situations is discussed. Some qualitative features of tunnelling with no magnetic interaction are retained, but some new ones are also observed. The resonance peaks in transmission spectrum generally do not reach 100% transmission probability when the magnetic field is turned on. We observe splitting and in some cases widening of transmission probability peaks. When the width b of area with magnetic field is large, we observe oscillations of spin-flip probability with energy and b which are caused by Larmor precession of spin about the vector of magnetic field. For some values of relevant parameters we also observe significant increase of tunnelling probability for low energies in the single particle case.

1. Introduction

Quantum tunnelling of systems with internal structure is a process that occurs frequently in many physical contexts. In case of particles without internal structure, resonant tunnelling through double-humped potential barrier is a well-known phenomenon with applications such as resonant tunnelling diodes. Tunnelling of two particles in a bound state was first studied by Zakhariiev and Sokolov [1]. Saito and Kayanuma [2] studied tunnelling of a two particles, with infinite square well binding potential, through a rectangular barrier, numerically and showed that resonant tunnelling of composite particles can occur in presence of a single potential barrier. Saito and Kayanuma also studied the tunnelling of a Wannier exciton through a single barrier heterostructure [3] and showed similar effects as in [2]. Their work has been expanded by investigating more general binding potentials and barriers by Pen'kov [4] [5], Flambaum and Zelevinsky [6], Goodvin and Shegelski [7] [8], and Bacca and Feldmeier [9]. Bertulani et al. [10] showed that tunnelling probability can be enhanced for systems with spin-like internal structure which can transition between states of different energy.

Examples of composite particle tunnelling phenomena are tunnelling of molecules [2] [7] [8] [11] [12] [13] [14] [15] [16] [17] [18], fusion of loosely-bound nuclei [19] [10] [20] [21] [6] [9], tunnelling of excitons [3] [22] [23] [24] and tunnelling of Cooper pairs [6]. There are experimental studies of exciton tunnelling which show that excitons tunnel as a whole [25] [26] and resonant tunnelling behaviour is also observed [26].

In this paper, we expand on previous works by considering tunnelling of composite particle with two internal degrees of freedom: binding interaction between the particles and spin. It can be expected that tunnelling of systems with two or more particles with spin, in presence of a magnetic field will occur in various situations, such as fusion of loosely-bound nuclei and tunnelling of excitons. Experimental studies of exciton tunnelling in presence of the magnetic field have already been conducted [27]. The objective of this paper is to investigate this phenomenon using a simple model, and to expand the existing results by examining the effects of an additional spin degree of freedom on composite particle tunnelling. In our model, we consider a one-dimensional two-particle system where one of the particles has spin $1/2$, tunnelling through a rectangular potential barrier. The interaction between particles is modelled as an infinite potential well, as in [2], while the magnetic field is homogeneous. Although the results are obtained within this simple model, we expect that their qualitative properties would be retained in a more sophisticated three-dimensional model with realistic binding potential, as in case of composite particle tunnelling without spin.

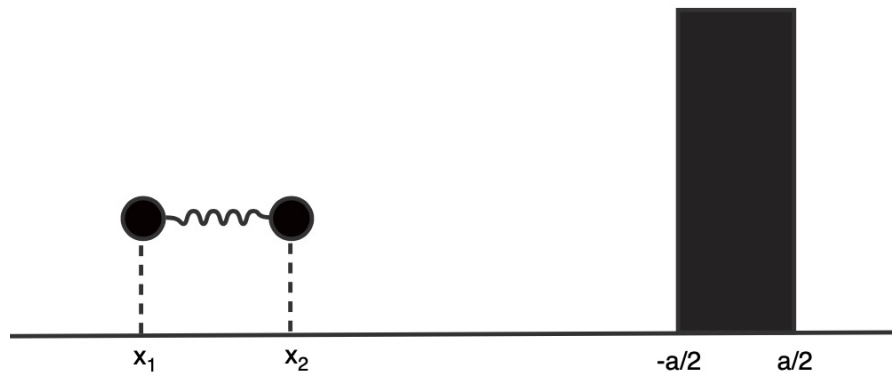


Fig. 1. Quantum tunnelling of a composite particle through a rectangular potential barrier

2. Description of the problem

As in Saito and Kayanuma [2] we consider a one dimensional two-particle system tunnelling through a rectangular barrier of width a , as in Figure 1. For a large enough barrier quantum tunnelling will occur with some probability which we will calculate. Each of the particles has a mass m and is point-like. One of the particles has spin $1/2$. The potential of intrinsic interaction is modelled as an infinite square potential well so the distance of the particles is confined in range $[l-d/2, l+d/2]$ with an average distance of l . The strength of binding can be controlled by the parameter d . The magnetic field is confined to a region of width b and has the same direction (the x -direction) as the velocity of the particle.

The interaction between particles is given as:

$$U(x) = \begin{cases} 0, & l - d/2 \leq x \leq l + d/2 \\ \infty, & \text{otherwise} \end{cases} \quad (1)$$

The potential barrier is defined as:

$$V(x) = \begin{cases} V_0, & |x| \leq a/2 \\ 0, & \text{otherwise} \end{cases} \quad (2)$$

The magnetic interaction is defined as:

$$f(x) = \begin{cases} u, & |x| \leq b \\ 0, & \text{otherwise} \end{cases} \quad (3)$$

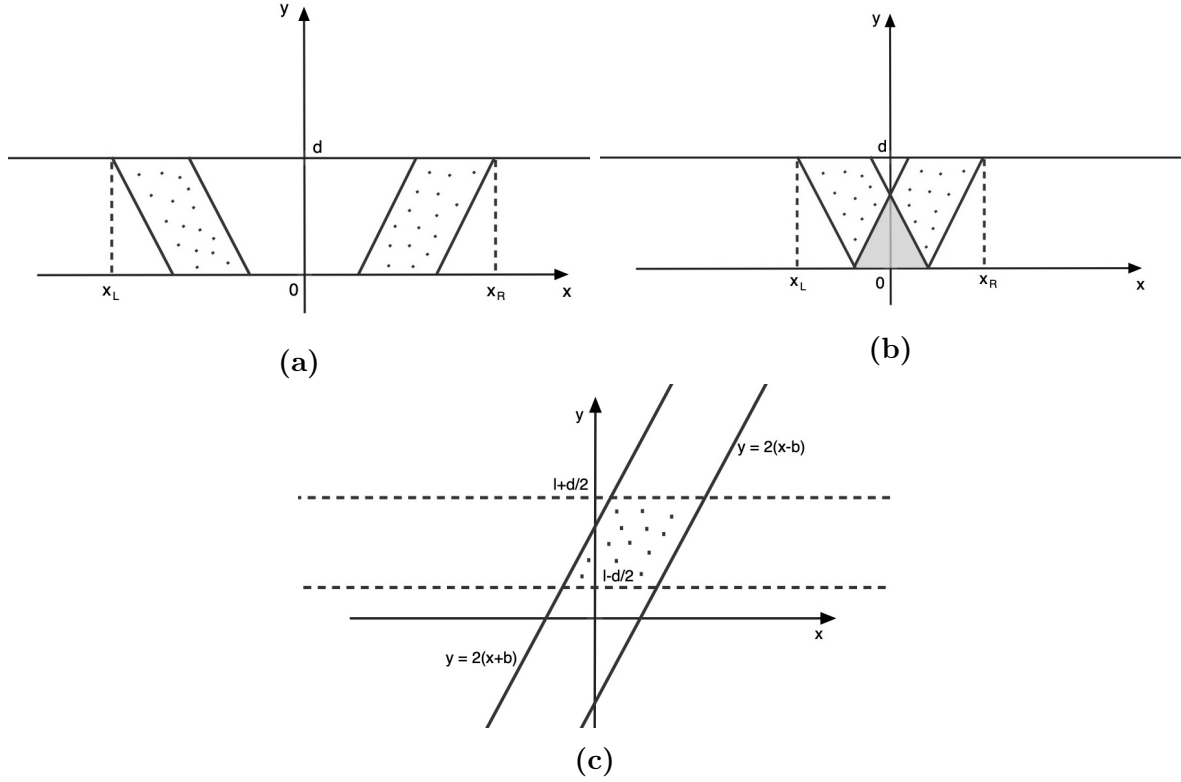


Fig. 2. Diagrams of the potential-barrier structure are shown in (a) and (b). For (a) $l - d/2 > a$ and (b) $l - d/2 < a$. In the dotted area in (a) $W(x, y) = V_0$, shaded area $W(x, y) = 2V_0$ and $W(x, y) = 0$ otherwise. $x_L = -(2a + 2l + d)/4$, $x_R = (2a + 2l + d)/4$. Diagram in (c) shows the structure of the magnetic interaction potential. In the dotted area of (c) $f(x - y/2) = \frac{2u}{d}$ and $f(x - y/2) = 0$ elsewhere.

The positions of particles are x_1 and x_2 . We define the centre of mass coordinate as $x = (x_1 + x_2)/2$ and the relative coordinate $y = x_2 - x_1 - l + d/2$. Now we can write the Hamiltonian of the system:

$$H = -\frac{\hbar^2}{4m} \frac{\partial^2}{\partial x^2} - \frac{\hbar^2}{m} \frac{\partial^2}{\partial y^2} + U(y) + V(x - y/2) + V(x + y/2) - f(x - y/2)\sigma_x \quad (4)$$

Tunnelling of a composite particle through a single square potential barrier is equivalent to successive tunnelling through two potential barriers [2]. The potential is equal to V_0 in the regions where $2x - a - l + d/2 \leq y \leq 2x + a - l + d/2$ and $-2x - a - l + d/2 \leq y \leq -2x + a - l + d/2$. Where these regions coalesce (which happens if $l - d/2 < a$) the potential is $2V_0$. We define the potential $W(x, y)$ with these properties.

Hence, the Schrödinger equation is written as:

$$-\frac{\hbar^2}{4m} \frac{\partial^2}{\partial x^2} \Psi(x, y) - \frac{\hbar^2}{m} \frac{\partial^2}{\partial y^2} \Psi(x, y) + U(y) \Psi(x, y) + W(x, y) \Psi(x, y) - f(x - y/2) \begin{pmatrix} 0 & 1 \\ 1 & 0 \end{pmatrix} \Psi(x, y) = E \Psi(x, y) \quad (5)$$

We now expand the wave function $\Psi(x, y)$ in the basis of spin in the z -direction and eigenfunctions of an infinite potential well:

$$\Psi(x, y) = \begin{pmatrix} \sum_{j=1}^{\infty} \psi_{j1}(x) \phi_{j1}(y) \\ \sum_{j=1}^{\infty} \psi_{j2}(x) \phi_{j2}(y) \end{pmatrix} = \sum_{j=1}^{\infty} \begin{pmatrix} \psi_{j1}(x) \\ \psi_{j2}(x) \end{pmatrix} \phi_j(y) \quad (6)$$

where

$$\phi_j(y) = \sqrt{\frac{2}{d}} \sin\left(\frac{j\pi}{d} y\right) \quad (7)$$

is the solution of the equation:

$$-\frac{\hbar^2}{m} \frac{d^2}{dy^2} \phi_j(y) = \varepsilon_j \phi_j(y) \quad (8)$$

with $\varepsilon_j = (\hbar/m)(j\pi/d)^2$ and the boundary condition $\phi_j(0) = \phi_j(d) = 0$.

By substituting the wave function in the Schrödinger equation by its expanded form, and then multiplying by ϕ_i^* , we obtain:

$$\sum_{j=1}^{\infty} -\frac{\hbar^2}{4m} \phi_i^* \phi_j \frac{d^2}{dx^2} \begin{pmatrix} \psi_{j1} \\ \psi_{j2} \end{pmatrix} - \frac{\hbar^2}{m} \begin{pmatrix} \psi_{j1} \\ \psi_{j2} \end{pmatrix} \phi_i^* \frac{d^2}{dy^2} \phi_j + \begin{pmatrix} \psi_{j1} \\ \psi_{j2} \end{pmatrix} \phi_i^* U(y) \phi_j + \begin{pmatrix} \psi_{j1} \\ \psi_{j2} \end{pmatrix} \phi_i^* W(x, y) \phi_j - \phi_i^* f(x - y/2) \begin{pmatrix} \psi_{j2} \\ \psi_{j1} \end{pmatrix} \phi_j = \sum_{j=1}^{\infty} E \begin{pmatrix} \psi_{j1} \\ \psi_{j2} \end{pmatrix} \phi_i^* \phi_j \quad (9)$$

We now integrate the whole equation from $-\infty$ to ∞ over the variable y and by using the orthonormality of eigenfunctions $\int_{-\infty}^{\infty} \phi_i^*(y) \phi_j(y) dy = \delta_{ij}$, we obtain the following equation by index:

$$-\frac{\hbar^2}{4m} \frac{d^2}{dx^2} \begin{pmatrix} \psi_{i1} \\ \psi_{i2} \end{pmatrix} + (\varepsilon_i - E) \begin{pmatrix} \psi_{i1} \\ \psi_{i2} \end{pmatrix} + \sum_{j=1}^{\infty} \begin{pmatrix} \psi_{j1} \\ \psi_{j2} \end{pmatrix} \int_{-\infty}^{\infty} \phi_i^* W(x, y) \phi_j dy - \sum_{j=1}^{\infty} \begin{pmatrix} \psi_{j2} \\ \psi_{j1} \end{pmatrix} \int_{-\infty}^{\infty} \phi_i^* f(x - y/2) \phi_j dy = \begin{pmatrix} 0 \\ 0 \end{pmatrix} \quad (10)$$

We now define the following functions:

$$W_{ij}(x) = \int_{-\infty}^{\infty} \phi_i^* W(x, y) \phi_j dy \quad (11)$$

$$F_{ij}(x) = \int_{-\infty}^{\infty} \phi_i^* f(x - y/2) \phi_j dy \quad (12)$$

Functions $W(x, y)$ and $f(x - y/2)$ are equal to zero outside of the regions $[0, d]$ and $[2(x - b), 2(x + b)]$ respectively. Thus, the real limits of the above integrals can be determined from Figures 2a and 2b for equation (11), and from Figure 2c for equation (8). After substituting the identity (7) into the equations, they can be solved analytically.

After some algebraic manipulation, and by defining the wave-number $k_j = 2\sqrt{m(E - \varepsilon_j)/\hbar}$, the equations become:

$$\frac{d^2}{dx^2} \begin{pmatrix} \psi_{i1} \\ \psi_{i2} \end{pmatrix} + k_j^2 \begin{pmatrix} \psi_{i1} \\ \psi_{i2} \end{pmatrix} - \frac{4m}{\hbar^2} \sum_{j=1}^{\infty} \begin{pmatrix} \psi_{j1} W_{ij}(x) - \psi_{j2} F_{ij}(x) \\ \psi_{j2} W_{ij}(x) - \psi_{j1} F_{ij}(x) \end{pmatrix} = \begin{pmatrix} 0 \\ 0 \end{pmatrix} \quad (13)$$

From now on we will call the k -th eigenstate of the internal mode channel k . So, for an incident wave with energy E , where $\varepsilon_n < E < \varepsilon_{n+1}$, propagating states in the region out of the potential barrier can exist for channels up to n (for both spin up and spin down states). The reflection amplitude R_{ln} and the transmission amplitude T_{ln} for the incident wave coming in channel n and going out in channel m are calculated using the Method of Variable Reflection Amplitude as shown in [28]. For an equation of the form:

$$\frac{d^2}{dx^2} \psi_n(x) + k_n^2 \psi_n(x) - \sum_{m=0}^{\infty} v_{nm}(x) \psi_m(x) = 0 \quad (14)$$

which can be easily adjusted to solve our vector equation (13), by defining the function $v_{nm}(x)$ accordingly and mapping the index m over both our pairs of indices $j1$ and $j2$, thus transforming our system of vector equations (defined by index) with equation (13), into a system of scalar equations and doubling their number.

If a plane wave form approaches the barrier from the left, in the l -th channel, the formal solution of the equation (14) is:

$$\psi_{ln}(x) = e^{ik_n x} \delta_{ln} + \sum_{m=0}^{\infty} \int_{-\infty}^{\infty} e^{ik_n |x-t|} v_{nm}(t) \psi_{lm}(t) dt \quad (15)$$

From [28], the reflection and transmission amplitudes can be written in the following form:

$$R_{ln} = \frac{1}{2ik_n} \sum_{m=0}^{\infty} \int_{-\infty}^{\infty} e^{ik_n t} v_{nm}(t) \psi_{lm}(t) dt \quad (16)$$

$$T_{ln} = \delta_{ln} + \frac{1}{2ik_n} \sum_{m=0}^{\infty} \int_{-\infty}^{\infty} e^{-ik_n t} v_{nm}(t) \psi_{lm}(t) dt \quad (17)$$

and further transformed into a system of differential equations:

$$\frac{d}{dx} R_{ln}(x) = - \sum_{j=0}^{\infty} \frac{1}{2ik_j} (e^{ik_j x} \delta_{jn} + R_{jn}(x) e^{-ik_j x}) \sum_{m=0}^{\infty} v_{jm}(x) (e^{ik_m x} \delta_{lm} + R_{lm}(x) e^{-ik_m x}) \quad (18)$$

$$\frac{d}{dx} T_{ln}(x) = - \sum_{j=0}^{\infty} \frac{1}{2ik_j} T_{jn}(x) e^{ik_j x} \sum_{m=0}^{\infty} v_{jm}(x) (e^{ik_m x} \delta_{lm} + R_{lm}(x) e^{-ik_m x}) \quad (19)$$

with the following boundary conditions:

$$R_{ln}(x \rightarrow \infty) \rightarrow 0, \quad R_{ln}(x \rightarrow -\infty) \rightarrow R_{ln} \quad (20)$$

$$T_{ln}(x \rightarrow \infty) \rightarrow \delta_{ln}, \quad T_{ln}(x \rightarrow -\infty) \rightarrow T_{ln} \quad (21)$$

By solving these equations for permitted channels (the sums will go from 0 to n instead of ∞) and in the specified range for the coordinate x (the centre of mass coordinate in range $[-(2a + 2l + d)/4, (2a + 2l + d)/4]$), the probability of reflection and transmission from channel l to channel n can be calculated as follows:

$$P_{r,l \rightarrow n} = \frac{k_n}{k_l} |R_{ln}(-\infty)|^2 \quad (22)$$

$$P_{t,l \rightarrow n} = \frac{k_n}{k_l} |T_{ln}(-\infty)|^2 \quad (23)$$

These expressions can be generalised to take into account the different spin states for each channel as explained before. Thus, there are $2n$ possible incoming states and $2n$ possible outgoing states, and the probabilities for every combination of those states can be calculated accordingly.

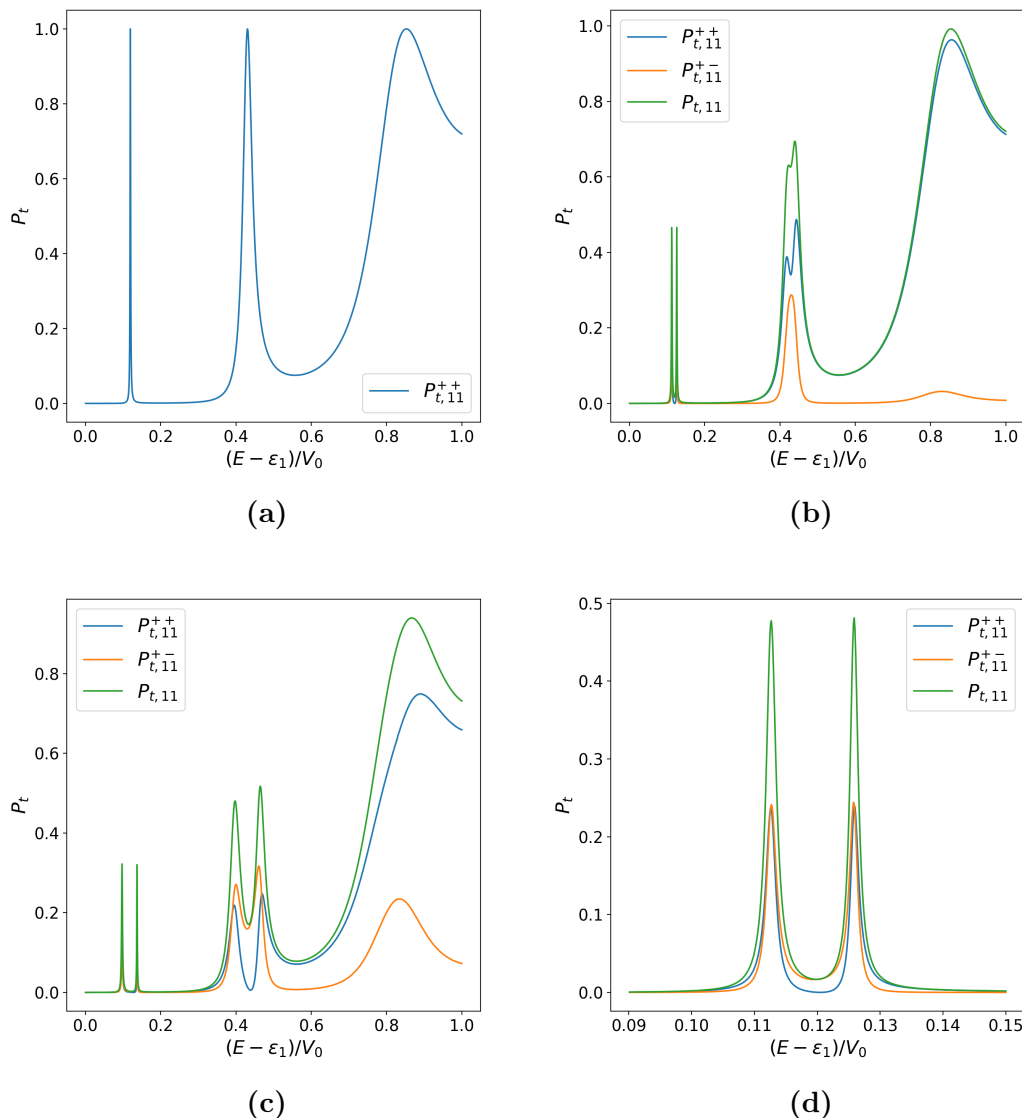


Fig. 3. The graphs show transmission probabilities from the first channel for $a = 1$, $b = 1$, $d = 5$, $l = 5$ and (a) $u = 0$, (b) $u = 0.05$, (c) $u = 0.15$, (d) $u = 0.05$. $P_{t,11}^{++}$ denotes a particle incoming in spin up state from channel 1 and outgoing in the same state, $P_{t,11}^{+-}$ denotes a particle incoming in spin up state from channel 1 and outgoing in spin down state. The probabilities $P_{t,11}^{--}$ and $P_{t,11}^{-+}$ are the same as $P_{t,11}^{++}$ and $P_{t,11}^{+-}$, respectively. The last graph shows the lowest energy peak of graph (b) in greater detail.

3. Results

Equations (18) and (19) are solved numerically using the Runge-Kutta method of order 8 for various values of parameters: width of the potential barrier a , strength of the magnetic field u and mean distance between the particles l , width of the potential well d and width of the area where the magnetic field is present b . In all cases we used fixed

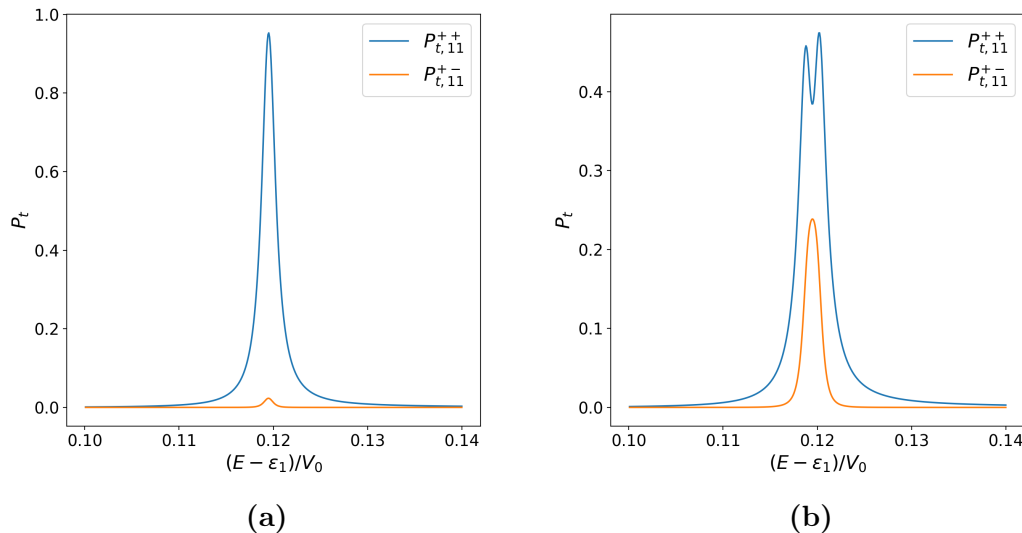


Fig. 4. The graphs show transmission probabilities around the lowest energy peak for the same parameters as in Figure 3a, except that for graph (a) $u = 0.001$ and for (b) $u = 0.005$.

values of parameters: $m = 1$, $\hbar = 1$, $V_0 = 1$. Python code that calculates transmission and reflection probabilities as functions of energy is provided in the appendix.

We checked the convergence of numerical results by reducing the maximum step used in the Runge-Kutta algorithm by a factor of 5. As expected, the results for spin up and spin down are symmetric and the sum of all probabilities of transmission and reflection for any given entry channel is 1.

In Figure 3a we reproduce one of the results shown in [2] when the magnetic field is absent, using the variable reflection amplitude method. In Figures 3b and 3c effects of the magnetic field are observed with other parameters kept the same as in Figure 3a. Resonances are wider and do not reach 100% transmission probability. It is visible that peaks are divided due to splitting of energy levels in presence of the magnetic field. This is more pronounced for the lowest energy peak. However, the splitting of the second peak is also clearly visible for stronger magnetic fields. As shown in Figure 3d spin transition is enhanced in the area of resonances.

In Figure 4 we examine the case of weak magnetic fields in the area of lowest energy resonance, with $b = a$. Bertulani et al. conclude in [10] that an extremely strong magnetic field is necessary to observe significant effects in the single particle case. If we examine composite particle tunnelling such effects are visible for much weaker fields in the area of resonances. In Figure 4a the lowest energy resonance peak at $u = 0.001$ already does not reach 100% transmission probability as it does when there is no magnetic field present in Figure 3a. Figure 4b shows that splitting of energy levels happens for magnetic fields as low as $u = 0.005$.

In Figure 5 we show the effect of varying width of the area where the magnetic field

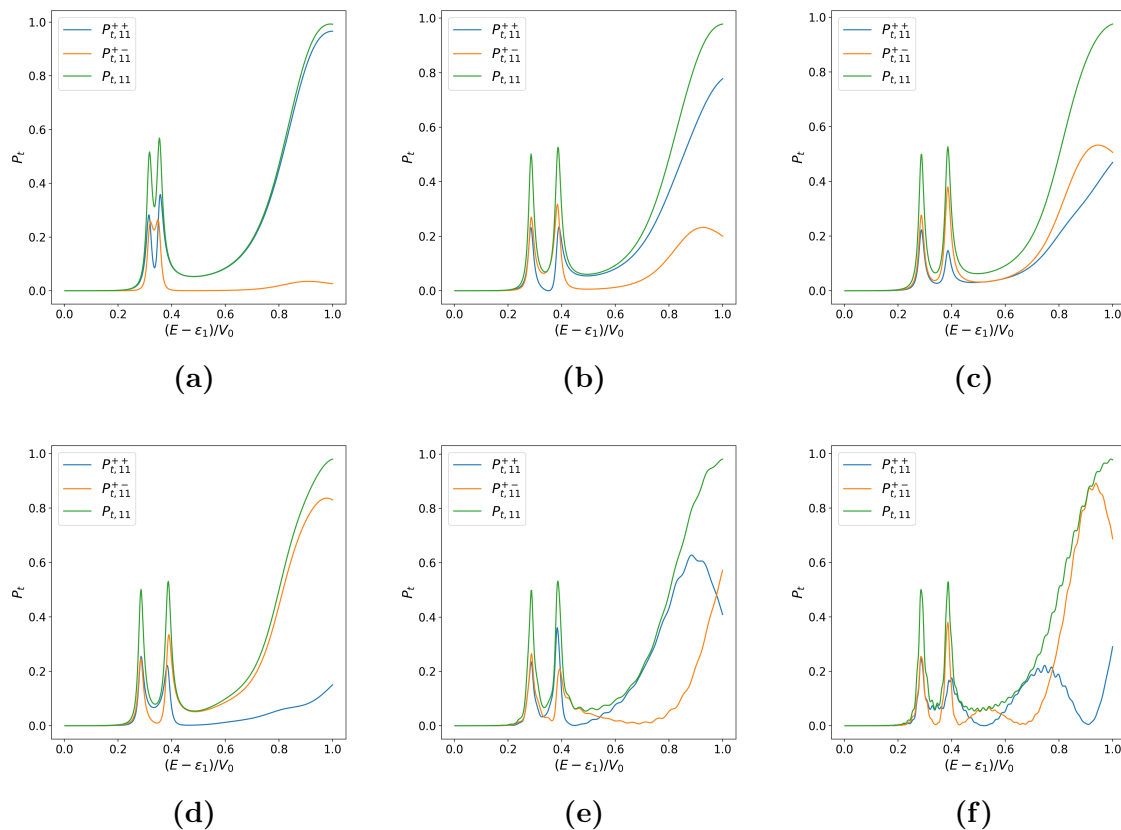


Fig. 5. The graphs show transmission probabilities from the first channel for $a = 1$, $d = 5$, $l = 3$, $u = 0.05$ and (a) $b = 1$, (b) $b = 3.5$, (c) $b = 8$, (d) $b = 15$, (e) $b = 100$, (f) $b = 200$.

is present. In the limit of small values of b the results tend towards the case when there is no magnetic field, i.e. the transmission probabilities $P_{t,ij}^{+-}$ tend to zero, which is to be expected. However, as can be seen from the progression of results in Figures 5a-5f, as the range of the field expands, $P_{t,ij}^{+-}$ and $P_{t,ij}^{++}$ exhibit oscillatory behaviour that will later be examined more closely. The graph of total transmission probability retains roughly the same shape. There are also smaller oscillations on the curves visible in Figures 5e and 5f.

In Figure 6 we can see a situation with multiple open channels. A discontinuity is observed in $P_{t,11}^{++}$ when the second channel becomes available. This is consistent with results from previous works [7]. We also observe that the total probability of transmission is reduced when higher channels open up, as in the case with no magnetic interaction [7].

In Figure 7 the case when the dimensions of the particle are smaller than dimensions of the barrier is examined. When l and a are of the same order of magnitude the effects of internal structure are clearly seen and in the case when $l \ll a$ the single particle limit is reproduced, as expected.

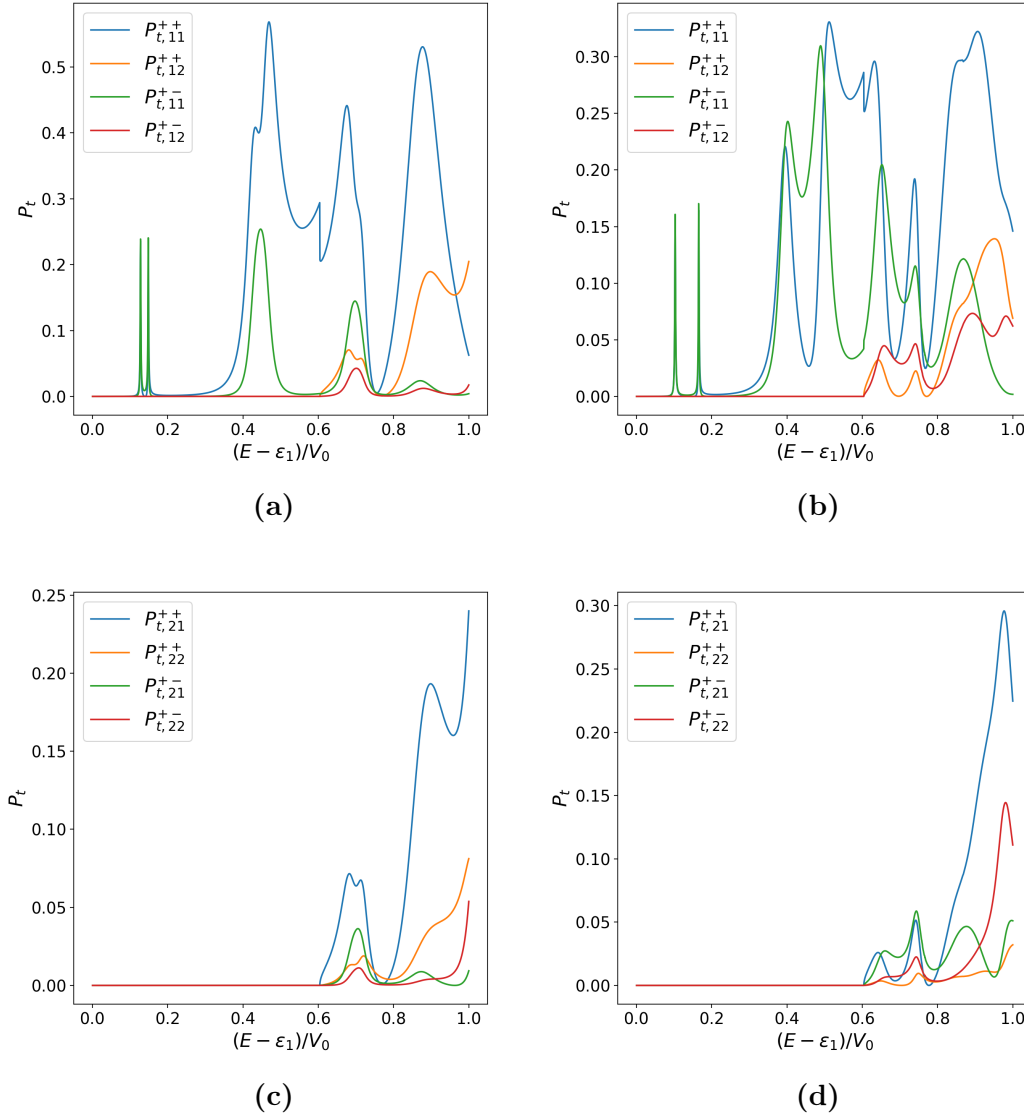


Fig. 6. The graphs show transmission probabilities for $a = 1$, $d = 7$, $l = 5$, $b = 1$ and (a) $u = 0.05$ from the first channel, (b) $u = 0.15$ from the first channel, (c) $u = 0.05$ from the second channel, (d) $u = 0.15$ from the second channel. The second channel opens at the energy of around 0.6 units for the given parameters.

In Figure 8 we show the effects of widening of the magnetic field in the single particle limit. There are two distinct oscillatory behaviours present for transmission probabilities with and without spin-flip, with respect to energy. The one with larger period doubles its frequency when the width of the field is doubled and this behaviour continues for every value of b . This effect can be explained by Larmor precession. Smaller oscillations also shorten their period when b increases. We can see that the overall transmission probability $P_{t,11} = P_{t,11}^{++} + P_{t,11}^{+-}$ remains roughly the same as in the single particle case (Figure 7b) invariant to b , except for the small oscillations visible

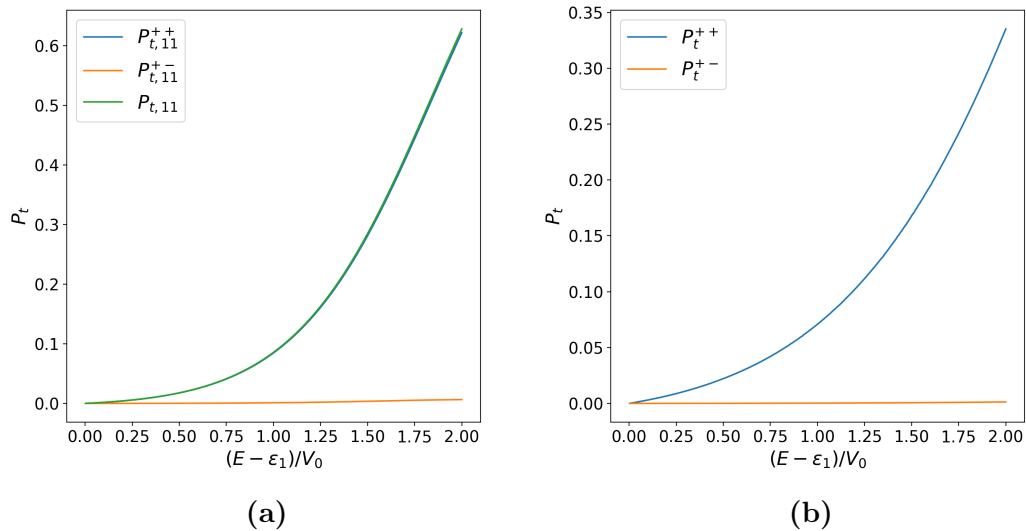


Fig. 7. The graphs show transmission probabilities from the first channel for $a = 1$, $b = 1$ (a) $d = 0.5$, $l = 0.5$, $u = 0.05$, (b) $d = 0.05$, $l = 0.05$, $u = 0.05$.

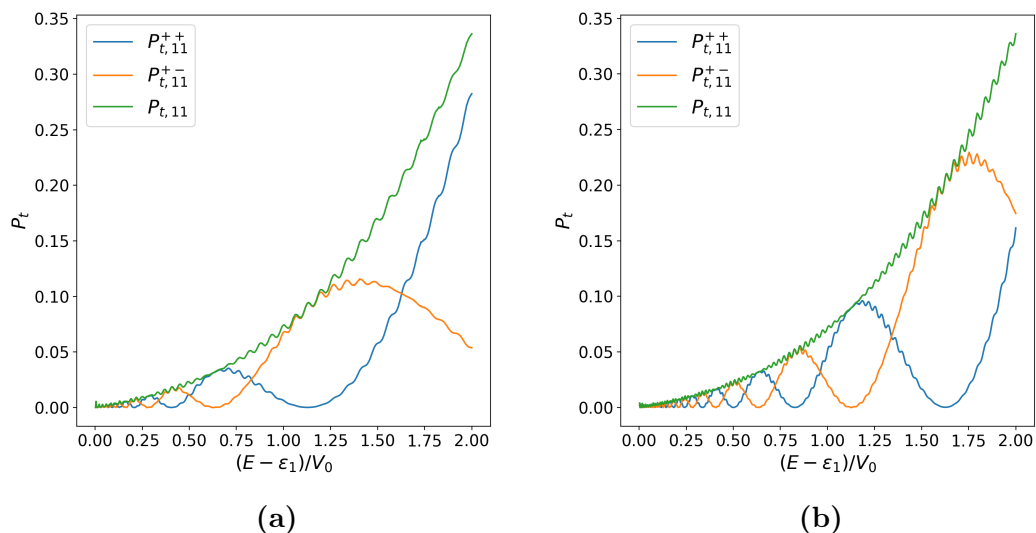


Fig. 8. The graphs show transmission probabilities from the first channel for $a = 1$, $u = 0.05$, $d = 0.05$, $l = 0.05$ (a) $b = 100$, (b) $b = 200$.

along the green line. There are also beats present in Figure 8b along the graph of total transmission probability which indicate a superposition of two oscillatory behaviours.

Finally, in Figure 9 we can see the remarkable properties of oscillatory behaviours in the single particle case when the ratio b/a is very large. There is a peak in total transmission probability for very low energies and it is not isolated, but accompanied by a large number of similar peaks, as shown in a more detailed look of the low energy region in Figure 9b. This behaviour, however is highly dependent upon the ratio b/a

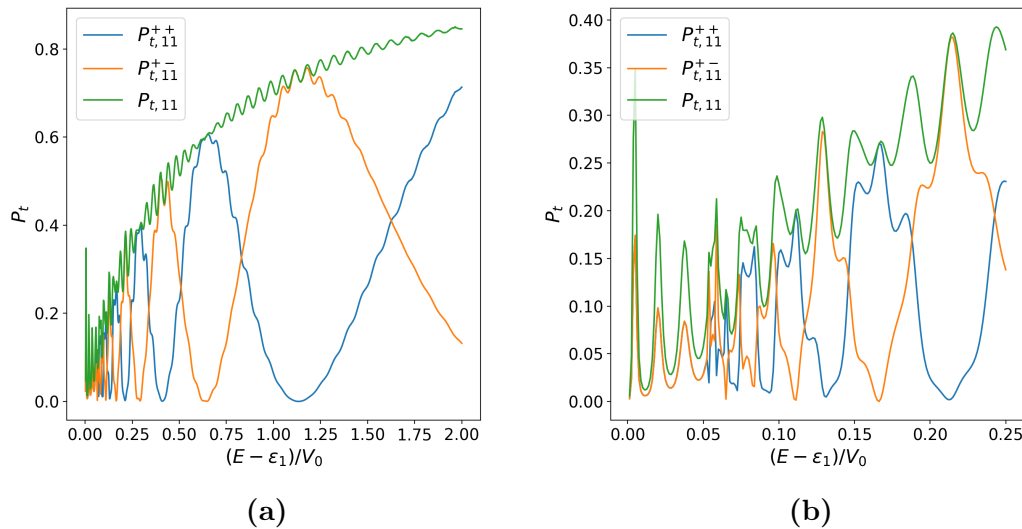


Fig. 9. The graphs show transmission probabilities from the first channel for $a = 0.3$, $u = 0.05$, $l = 0.05$, $d = 0.05$, $b = 100$ for different energy ranges.

and is not always enhanced by increasing it, however, for lower values it is always less pronounced.

4. Discussion

The results show that the additional magnetic interaction has several noticeable effects on tunnelling probability. When dimensions of the composite particle are larger than dimensions of the barrier, the effects of magnetic field and spin are most clearly observed around the transmission probability resonances. In case with no magnetic field, the resonances reach 100% transmission probability, which is no longer the case when the magnetic field is turned on. Also, with the magnetic field present, the resonance peaks split and each forms two peaks close to each other. The structure of these peaks is generally nearly symmetric and depends on values of parameters u and b , as seen in Figures 3, 5 and 6a. In realistic physical situations we can expect that the interaction with magnetic field will either be present in the whole space, i.e. an area much larger than the potential barrier, or localised in the area of the potential barrier.

When we set the width of area with magnetic field $b = a \sim 1$, effects of magnetic field are relatively small for field strengths $u < 10^{-2}V_0$, which can be expected in most situations. The splitting of transmission probability peaks can be observed if $u \sim 10^{-2}V_0$ or larger, but even with $u \sim 10^{-3}V_0$ the lowest energy transmission probability peak no longer reaches 1. Probability of transmission with spin-flip P_t^{+-} is much larger relatively to P_t^{++} in the resonance area. With the opening of higher channels, the structure of plots becomes more complicated, but no qualitatively new effects are observed.

In cases with $l < a$, the magnetic field has small effects on total tunnelling

probability, except for very large values of $u \sim V_0$ which are not realistic, or very large values of b . Generally, the effects of magnetic field are more pronounced for smaller values of a which is expected because when the barrier is smaller, small splitting of energy levels becomes more important. The effects of internal structure are observed when $l < a$ if l and a are of the same order of magnitude because the effective barrier as seen by particle's centre of mass is different than in the single particle case: the barrier effectively becomes wider and lower.

If the magnetic field is present in a wide area ($b \gg a$), several interesting effects can be seen. The effects of magnetic interaction can be observed with field strength which is an order of magnitude smaller than in case $b = a$. The splitting of resonances becomes more pronounced, and the new peaks are farther apart on the energy scale. Energy difference between the peaks is approximately $2u$, which is equal to the energy difference between the eigenstates of spin in the x -direction. Total transmission probability does not change significantly compared to the case when $b = a$, but probability of spin-flip does. When we calculate transmission and reflection probabilities for large values of b , the obtained results do not converge to a constant value for each probability with given parameters. Instead, the results for P_t^{++} and P_t^{+-} exhibit a sort of oscillatory behaviour when we examine the results for different values of parameter b , as seen in Figures 5, 8 and 9. This behaviour is observed even more clearly when we examine the single particle limit, with $l \ll a$. In that limit, the oscillations of spin-flip probability with energy are also clearly seen. An additional effect possible for some values of parameters in the single particle case is seen in Figure 9 where we observe multiple transmission probability peaks in the low energy range which can significantly increase the total tunnelling probability.

Perhaps the most interesting effect of magnetic interaction are these oscillations of spin-flip probability. They are caused by Larmor precession of spin. We expanded the composite particle spin in the σ_z eigenbasis, and the magnetic field is pointing in x -direction. Because of that choice, we can set $\vec{A} = 0$ along the path of composite particle which simplifies the Schrödinger equation, and we also have transitions from spin-up to spin-down state and vice versa. Spin-up and spin-down states in z -direction are not the eigenstates of σ_x , so Larmor precession of spin happens when the magnetic field is present. We solved the time-independent Schrödinger equation, but we can always think of its solution as a limit of a time-dependent wave packet initially travelling in $+x$ -direction incident on a potential barrier and area with magnetic field. It is clear that the total angle of spin rotation is proportional to time spent in the area with magnetic field, which means it is proportional to b when $b \gg a$, i.e. the only interaction is magnetic and kinetic energy are constant for most of the time spent travelling through the field. Also, for different energies, time of travel through the area with field is different, so the total angle of rotation is different. A nice confirmation of this is halving of the "period" of oscillations in energy when b is doubled in the single particle case, as seen in Figure 8.

We give no direct explanation for smaller oscillations seen in Figures 5e, 5f, 8 and

9. They appear when the ratio of width of magnetic field and width of potential barrier becomes large enough, roughly of the order of magnitude 10^2 , and when other effects (i.e. resonant tunnelling) become less noticeable. Hence, they are best visible in the single particle limit, but can also appear when the compositeness of the particle is relevant (Figures 5e and 5f). In some cases, those oscillations can significantly influence total tunnelling probability as showed in Figure 9. This behaviour is reminiscent of some sort of "nutation" superposed on Larmor precession, however, this effect is yet to be studied more closely.

We also see that the effects of magnetic interaction are the greatest around transmission resonances. In some cases, apart from splitting, widening of resonances is also observed. The most likely explanation for this is that the coupling between the magnetic interaction, the internal interaction of the particle (infinite potential well in this case) and the interaction with potential barrier has the strongest effects when the coupling between the latter two interactions produces transmission resonances.

As noted in the introduction, tunnelling of composite particles occurs in various physical contexts, and this simple model should be qualitatively applicable to those situations where splitting of energy levels in magnetic field is large enough. If we take a particle with magnetic moment μ_B as an example, with V_0 and a of order 10^{-1} eV and nm, respectively, for magnetic field strength of 1 T we get $u \sim 10^{-4}$ eV. This means that the effects of magnetic field presence could be observable for realistic field strengths and barriers for particles with large enough magnetic moment, for example in experiments with exciton tunnelling and possibly in some molecule tunnelling situations. The effects should be more apparent if splitting of energies is very large, example of which is the giant Zeeman effect.

5. Conclusion

We have studied tunnelling of a composite particle in presence of a magnetic field. The exact numerical solution is provided within the context of a simple model we used. Further work could include studying more realistic binding potentials, three-dimensional version of the problem, and magnetic field pointing in a general direction. These expansions would make the problem significantly more complicated because orbital angular momentum and presence of a magnetic vector potential would have to be taken into account. However, we expect that qualitative features of our results would be retained as shown in e.g. [8] for the case of composite particle tunnelling with no magnetic field, but it is also possible that additional degrees of freedom would significantly alter the results. Effects originating from Larmor precession and splitting of energy levels in magnetic field would certainly be present in more realistic models, but because of complexity of the results it is hard to predict whether additional translational and rotational degrees of freedom would result in some new effects which are not present in our one-dimensional case. A topic of further research could also be the explanation of smaller oscillations which are noticed when $b \gg a$.

This work shows that, based on results obtained within a simple framework, the main effects of additional magnetic interaction on composite particle tunnelling are splitting and in some cases widening of resonance transmission probability peaks which do not reach 100% transmission probability when the magnetic field is turned on, and oscillations of spin-flip probability with energy and width of the magnetic field. It can also be expected that these effects could be observed in realistic experiments with exciton tunnelling, where composite particle tunnelling in presence of a magnetic field has already been studied. When the splitting of energy levels caused by magnetic field is more than 4 orders of magnitude smaller than barrier height, with realistic barrier widths, the magnetic interaction can be neglected, which would be the case in situations from nuclear physics.

We have also given a physical explanation for the fact that probabilities of transmission P_t^{++} and P_t^{+-} do not converge to a single value in the limit $b \gg a$. It is interesting that spin-flip probability depends strongly on width of an area with magnetic field presence, independently of ratio b/a . This is a clear manifestation of Larmor precession in a time-independent model. The splitting of transmission probability peak is expected as a consequence of splitting of energy levels in a magnetic field. The fact that new peaks do not reach 100% transmission probability can be explained as a consequence of the specific nature of coupling between magnetic interaction with other interactions, so the conditions for 100% transmission probability are no longer satisfied when it is present.

Acknowledgements

We would like to thank M. Milin, also M. T. Cvitaš from the University of Zagreb and K. Pisk from Ruđer Bošković Institute for useful discussions and comments.

6. Appendix

6.1. Python code for generating graphs seen in the figures

```

from scipy.integrate import solve_ivp
import math
import cmath
import matplotlib.pyplot as plt
import numpy as np

a = 1.
b = 1.
d = 5.
l = 5.
u = 0.05
dot = 800
ran = 1

h = 1.
m = 1.
V0 = 1.
konst = (4 * m / (h * h))

def W_funk(W0, g1, g2, n1, n2):
    if n1 == n2:
        return W0 * ((g2 / d) - (1 / (n1 * math.pi))) * (
            math.sin(n1 * math.pi * g2 / d) *
            math.cos(n1 * math.pi * g2 / d))) - W0 * (
                (g1 / d) - (1 / (n1 * math.pi))) * (
                    math.sin(n1 * math.pi * g1 / d) *
                    math.cos(n1 * math.pi * g1 / d)))
    else:
        return (W0 / (math.pi * (n1 - n2))) * (
            math.sin((math.pi * (n1 - n2) * g2) / d) -
            math.sin((math.pi * (n1 - n2) * g1) / d)) - (
                W0 / (math.pi * (n1 + n2))) * (
                    math.sin((math.pi * (n1 + n2) * g2) / d) -
                    math.sin((math.pi * (n1 + n2) * g1) / d))

```

```

def W(cnt1, cnt2, y):
    y1 = 2 * y - a - l + d / 2
    y2 = 2 * y + a - l + d / 2
    y3 = -2 * y - a - l + d / 2
    y4 = -2 * y + a - l + d / 2
    Y = [y1, y2, y3, y4]
    for pom in range(4):
        if Y[pom] < 0: Y[pom] = 0
        if Y[pom] > d: Y[pom] = d
    W = 0
    if Y[0] == Y[1] and Y[2] == Y[3]:
        W = 0
    elif Y[0] == Y[1]:
        W = W_funk(V0, Y[2], Y[3], cnt1 + 1, cnt2 + 1)
    elif Y[2] == Y[3]:
        W = W_funk(V0, Y[0], Y[1], cnt1 + 1, cnt2 + 1)
    elif Y[0] == Y[2] and Y[1] == Y[3]:
        W = W_funk(2 * V0, Y[0], Y[1], cnt1 + 1, cnt2 + 1)
    elif (Y[1] > Y[0] >= Y[3] > Y[2]) or (Y[3] > Y[2] >= Y[1] > Y[0]):
        W = W_funk(V0, Y[0], Y[1], cnt1 + 1, cnt2 + 1) +
            W_funk(V0, Y[2], Y[3], cnt1 + 1, cnt2 + 1)
    elif Y[1] >= Y[3] > Y[0] >= Y[2]:
        W = W_funk(2 * V0, Y[0], Y[3], cnt1 + 1, cnt2 + 1) +
            W_funk(V0, Y[3], Y[1], cnt1 + 1, cnt2 + 1) +
            W_funk(V0, Y[2], Y[0], cnt1 + 1, cnt2 + 1)
    elif Y[3] >= Y[1] > Y[2] >= Y[0]:
        W = W_funk(2 * V0, Y[2], Y[1], cnt1 + 1, cnt2 + 1) +
            W_funk(V0, Y[1], Y[3], cnt1 + 1, cnt2 + 1) +
            W_funk(V0, Y[0], Y[2], cnt1 + 1, cnt2 + 1)
    return W

```

```

def F_funk(cnt1, cnt2, y):
    f = 0

    if (1 - d / 2) < 2 * (y - b) < 2 * (y + b) < (1 + d / 2):
        f += W_funk(u, 2 * (y - b), 2 * (y + b), cnt1 + 1, cnt2 + 1)
    elif (1 - d / 2) < 2 * (y - b) < (1 + d / 2) < 2 * (y + b):
        f += W_funk(u, 2 * (y - b), (1 + d / 2), cnt1 + 1, cnt2 + 1)
    elif 2 * (y - b) < (1 - d / 2) < 2 * (y + b) < (1 + d / 2):

```

```

    f += W_funk(u, (1 - d / 2), 2 * (y + b), cnt1 + 1, cnt2 + 1)
elif 2 * (y - b) < (1 - d / 2) < (1 + d / 2) < 2 * (y + b):
    f += W_funk(u, (1 - d / 2), (1 + d / 2), cnt1 + 1, cnt2 + 1)

return f

```

```

def G(cnt1, cnt2, y):
    if cnt1 < c and cnt2 < c:
        return konst * W(cnt1, cnt2, y)
    if cnt1 < c <= cnt2:
        return -konst * F_funk(cnt1, cnt2 - c, y)
    if cnt1 >= c > cnt2:
        return -konst * F_funk(cnt1 - c, cnt2, y)
    if cnt1 >= c and cnt2 >= c:
        return konst * W(cnt1 - c, cnt2 - c, y)

```

```

def sys(y, R):
    F = [0j] * 8 * c * c

    Fa = np.array(F)
    Ra = np.array(R)

    Rm = Ra.reshape(4 * c, 2 * c)
    Fm = Fa.reshape(4 * c, 2 * c)

    y1 = 2 * y - a - l + d / 2
    y2 = 2 * y + a - l + d / 2
    y3 = -2 * y - a - l + d / 2
    y4 = -2 * y + a - l + d / 2
    Y = [y1, y2, y3, y4]
    for pom in range(4):
        if Y[pom] < 0: Y[pom] = 0
        if Y[pom] > d: Y[pom] = d

    for i in range(2 * c):
        for j in range(2 * c):
            for cnt1 in range(2 * c):
                konst1 = (-1 / (2j * k[cnt1 % c]))
                konst2 = cmath.exp(-1j * k[cnt1 % c] * y)
                konst3 = cmath.exp(1j * k[cnt1 % c] * y)

```

```

for cnt2 in range(2 * c):
    konst4 = cmath.exp(-1j * k[cnt2 % c] * y)
    konst5 = cmath.exp(1j * k[cnt2 % c] * y)

    Fm[i][j] += konst1 * (konst3 * (i == cnt1) + konst2 *
        Rm[i][cnt1]) * (G(cnt1, cnt2, y) * (
            konst5 * (j == cnt2) + konst4 * Rm[cnt2][j]))

    Fm[2 * c + i][j] += konst1*(konst2 * Rm[2 * c + i][cnt1]) *
        (G(cnt1, cnt2, y) * (
            konst5 * (j == cnt2) + konst4 * Rm[cnt2][j]))

return Fm.flatten()

```

```

Tgg11 = [0] * dot
Tgg12 = [0] * dot
Tgd11 = [0] * dot
Tgd12 = [0] * dot
T11 = [0] * dot
en = [0] * dot
uk = [0] * dot

```

```

for cnt in range(dot):
    n = 7
    c = 0

```

$$E = (h * h * \text{math.pi} * \text{math.pi} / (m * d * d)) + (cnt + 1) * \text{ran} * V0 / \text{dot}$$

$$xl = -1 * (2 * \text{max}(b, a) + 2 * l + d) / 4$$

$$xr = (2 * \text{max}(b, a) + 2 * l + d) / 4$$

```

ep = [0] * n
k = [0] * n

```

```

for i in range(1, n + 1):
    ep[i - 1] = h * h * i * i * \text{math.pi} * \text{math.pi} / (m * d * d)
    if ep[i - 1] < E:
        c = i
        k[i - 1] = (2 / h) * \text{math.sqrt}(m * (E - ep[i - 1]))

```

$$\text{en}[cnt] = (E - \text{ep}[0]) / V0$$

```

init_ar = np.zeros(8 * c * c) + 0j

init_m = init_ar.reshape(4 * c, 2 * c)

for red in range(2 * c):
    init_m[2 * c + red][red] += 1

init = init_m.flatten()

res = solve_ivp(sys, (xr, xl), init, method='DOP853', max_step=0.3)
f_moment = len(res.t) - 1

res_f = [0j] * len(res.y)
for pom in range(len(res.y)):
    res_f[pom] += res.y[pom][f_moment]

res_a = np.array(res_f)
res_m = res_a.reshape(4 * c, 2 * c)

Tgg11[cnt] += abs(res_m[2 * c][0]) * abs(res_m[2 * c][0])
if c > 1:
    Tgd11[cnt] += abs(res_m[2 * c + 2][0]) *
    abs(res_m[2 * c + 2][0])
    Tgg12[cnt] += abs(res_m[2 * c + 1][0]) *
    abs(res_m[2 * c + 1][0]) * k[1] / k[0]
    Tgd12[cnt] += abs(res_m[2 * c + 3][0]) *
    abs(res_m[2 * c + 3][0]) * k[1] / k[0]
else:
    Tgd11[cnt] += abs(res_m[2 * c + 1][0]) *
    abs(res_m[2 * c + 1][0])

T11[cnt] = Tgd11[cnt] + Tgg11[cnt]

for pom in range(2 * c):
    uk[cnt] += k[pom % c] / k[0] * (abs(res_m[pom][0]) *
    abs(res_m[pom][0]) + abs(
    res_m[2 * c + pom][0]) * abs(res_m[2 * c + pom][0]))

print(cnt)

fig, ax = plt.subplots(figsize=[7, 7])
plt.plot(en, Tgg11, label=r'$P_{t,11}^{++}$')

```

```

plt.plot(en, Tgg12, label=r'$P_{t,12}^{\{++\}}$')
plt.plot(en, Tgd11, label=r'$P_{t,11}^{\{+-\}}$')
plt.plot(en, Tgd12, label=r'$P_{t,12}^{\{+-\}}$')
# plt.plot(en, T11, label=r'$P_{t,11}$')
# plt.plot(en, uk, label="uk")

plt.xlabel(r'$\epsilon_1/V_0$', fontsize=18)
plt.ylabel(r'$P_t$', fontsize=18)
plt.xticks(fontsize=15)
plt.yticks(fontsize=15)
plt.legend(fontsize=18)
plt.show()

```

References

1. B.N., Z. & S.N., S. Metastable States of a Coupled Pair on a Repulsive Barrier. *Annalen der Physik* **469**, 229–232 (1964).
2. Saito, N. & Kayanuma, Y. Resonant tunnelling of a composite particle through a single potential barrier. *Journal of Physics: Condensed Matter* **6**, 3759–3766 (1994).
3. Saito & Kayanuma. Resonant tunneling of a Wannier exciton through a single-barrier heterostructure. *Physical review. B, Condensed matter* **51** **8**, 5453–5456 (1995).
4. Pen'kov, F. Metastable States of a Coupled Pair on a Repulsive Barrier. *Physical Review A* **62** (Apr. 2000).
5. Pen'kov, F. M. Quantum transmittance of barriers for composite particles. *Journal of Experimental and Theoretical Physics* **91**, 698–705 (2000).
6. Flambaum, V. V. & Zelevinsky, V. Quantum tunnelling of a complex system: effects of a finite size and intrinsic structure. *Journal of Physics G* **31**, 355–360 (2005).
7. Goodvin, G. L. & Shegelski, M. R. A. Tunneling of a diatomic molecule incident upon a potential barrier. *Physical Review A* **71**, 032719 (2005).
8. Goodvin, G. L. & Shegelski, M. R. A. Three-dimensional tunneling of a diatomic molecule incident upon a potential barrier. *Phys. Rev. A* **72**, 042713. <https://link.aps.org/doi/10.1103/PhysRevA.72.042713> (4 Oct. 2005).
9. Bacca, S. & Feldmeier, H. Resonant tunneling in a schematic model. *Phys. Rev. C* **73**, 054608. <https://link.aps.org/doi/10.1103/PhysRevC.73.054608> (5 May 2006).
10. Bertulani, C. A., Flambaum, V. V. & Zelevinsky, V. G. Tunneling of a composite particle: effects of intrinsic structure. *Journal of Physics G: Nuclear and Particle Physics* **34**, 2289–2295. <https://doi.org/10.1088%2F0954-3899%2F34%2F11%2F006> (Oct. 2007).

11. Shegelski, M. R. A. & Jones, G. Resonant transmission of a weakly bound molecule incident upon a step potential. *Journal of Physics B* **49**, 165101 (2016).
12. Shegelski, M. R. A., Pittman, J. T., Vogt, R. E., Kavka, J. & Mandy, M. E. Tunnelling of a molecule with many bound states in three dimensions. *Journal of Physics B* **46**, 045201 (2013).
13. Shegelski, M. R. A. & Jones, G. Resonant transmission of a weakly bound molecule incident upon a step potential. *Journal of Physics B* **49**, 165101 (2016).
14. Shegelski, M. R. A., Jones, G., Sample, C. M., Hawse, M. & Reid, M. Resonant transmission of weakly bound multi-atomic molecules. *Journal of Physics B: Atomic, Molecular and Optical Physics* (2019).
15. Krassovitskiy, P. & Pen'kov, F. M. Resonance diffusion of beryllium molecule. *Bulletin of the Russian Academy of Sciences: Physics* **79**, 930–934 (2015).
16. Krassovitskiy, P. & Pen'kov, F. M. Contribution of resonance tunneling of molecule to physical observables. *Journal of Physics B* **47**, 225210 (2014).
17. Krassovitskiy, P. & Pen'kov, F. M. Phase analysis for the transmission of a coupled pair through the potential barrier and reflecting off it. *Bulletin of the Russian Academy of Sciences: Physics* **80**, 338–342 (2016).
18. Vinitzky, S. I. *et al.* Models of quantum tunneling of a diatomic molecule affected by laser pulses through repulsive barriers in Saratov Fall Meeting (2014).
19. Kimura, S. & Takigawa, N. Fusion from an excited state. *Phys. Rev. C* **66**, 024603. <https://link.aps.org/doi/10.1103/PhysRevC.66.024603> (2 Aug. 2002).
20. Ahsan, N. & Volya, A. Quantum tunneling and scattering of a composite object reexamined. *Phys. Rev. C* **82**, 064607. <https://link.aps.org/doi/10.1103/PhysRevC.82.064607> (6 Dec. 2010).
21. Shotter, A. C. & Shotter, M. D. Quantum mechanical tunneling of composite particle systems: Linkage to sub-barrier nuclear reactions. *Phys. Rev. C* **83**, 054621. <https://link.aps.org/doi/10.1103/PhysRevC.83.054621> (5 May 2011).
22. Kavka, J., Shegelski, M. R. A. & Hong, W.-p. Tunneling and reflection of an exciton incident upon a quantum heterostructure barrier. *Journal of physics. Condensed matter : an Institute of Physics journal* **24** **36**, 365802 (2012).
23. Guzun, D. *et al.* Effect of resonant tunneling on exciton dynamics in coupled dot-well nanostructures. *Journal of Applied Physics* **113**, 154304 (2013).
24. Kilcullen, P., Ladouceur, L., Malmgren, K., Reid, M. & Shegelski, M. One Dimensional Time-Dependent Tunnelling of Excitons. *Few-Body Systems* **58** (Jan. 2017).
25. Lawrence *et al.* Exciton tunneling revealed by magnetically tuned interwell coupling in semiconductor double quantum wells. *Physical review letters* **73** **15**, 2131–2134 (1994).

26. Haacke, S. *et al.* Tunneling dynamics in CdTe/(Cd,Zn)Te asymmetric double-quantum-well structures. *Phys. Rev. B* **47**, 16643–16646. <https://link.aps.org/doi/10.1103/PhysRevB.47.16643> (24 June 1993).
27. Zaitsev, S. V., Brichkin, A. S., Dorozhkin, P. S. & Bacher, G. Relaxation of excitons in semimagnetic asymmetric double quantum wells. *Semiconductors* **42**, 813–827 (2008).
28. Razavy, M. *Quantum Theory of Tunnelling* ISBN: 9812380183 (World Scientific Publishing, 2003).